Structural Basis for Catalytic Activity and Enzyme Polymerization of Phospholipid Hydroperoxide Glutathione Peroxidase-4 (GPx4)[†,‡,§]

Patrick Scheerer, Astrid Borchert, Norbert Krauss, Helga Wessner, Christa Gerth, Wolfgang Höhne, and Hartmut Kuhn*

Institute of Biochemistry, University Medicine Berlin−Charité, Monbijoustr. 2, D-10117 Berlin, Germany

Received May 4, 2007; Revised Manuscript Received June 4, 2007

ABSTRACT: Phospholipid hydroperoxide glutathione peroxidase (GPx4) is a moonlighting selenoprotein, which has been implicated in anti-oxidative defense, sperm development, and cerebral embryogenesis. Among GPx-isoforms, GPx4 is unique because of its capability to reduce complex lipid hydroperoxides and its tendency toward polymerization, but the structural basis for these properties remained unclear. To address this, we solved the crystal structure of the catalytically active U46C mutant of human GPx4 to 1.55 Å resolution. X-ray data indicated a monomeric protein consisting of four α-helices and seven β-strands. GPx4 lacks a surface exposed loop domain, which appears to limit the accessibility of the active site of other GPx-isoforms, and these data may explain the broad substrate specificity of GPx4. The catalytic triad (C46, Q81, and W136) is localized at a flat impression of the protein surface extending into a surface exposed patch of basic amino acids (K48, K135, and R152) that also contains polar T139. Multiple mutations of the catalytic triad indicated its functional importance. Like the wild-type enzyme, the U46C mutant exhibits a strong tendency toward protein polymerization, which was prevented by reductants. Site-directed mutagenesis suggested involvement of the catalytic C46 and surface exposed C10 and C66 in polymer formation. In GPx4 crystals, these residues contact adjacent protein monomers.

Glutathione peroxidases (GPx[1]) are part of the cellular anti-oxidative defense system (*1*) and catalyze the reduction of hydroperoxides at the expense of reduced glutathione and/or other reductants. There are selenium-containing and selenium-free glutathione peroxidases. Mammalian selenium GPx-isoforms (*2*) have been classified in several subfamilies, which are numbered consecutively (GPx1 to GPx7). Among the GPx-isoforms, phospholipid hydroperoxide glutathione peroxidase (GPx4) is somewhat unique because of its capability to accept complex hydroperoxy lipids as substrate, its strong tendency toward protein polymerization, and its multiple biological functionality (*3*). As an enzymatic antioxidant (*2*, *3*), it is capable of reducing a large array of hydroperoxy lipids including peroxidized phospholipids and cholesterol esters (*4*). In addition, the enzyme has been implicated as structural protein in sperm maturation (*5*) and appears to be involved in the regulation of apoptosis (*6*). More recent data suggested its importance for cerebral embryogenesis (*7*). The human GPx4 gene is located on chromosome 19, and three different GPx4 variants (cytosolic isoform (c-GPx4), mitochondrial isoform (m-GPx4), and nuclear isoform (n-GPx4)) originate from this gene (*2*, *3*). These enzyme variants are expressed at low levels in most mammalian cells, but large amounts have been detected in the testis (*2*). Low testicular levels of GPx4 have been related to male infertility (*8*), but these alterations could not be linked to naturally occurring mutations in the GPx4 gene (*9*).

Cytosolic GPx4 (c-GPx4) is a single polypeptide chain protein with a molecular mass of 19.5 kDa, which does not undergo major post-translational modification (*10*). Amino acid 46 is a selenocysteine (U46) that is encoded by the TGA opal codon. Premature translational termination is prevented by the selenocysteine insertion sequence localized in the 3′-untranslated region of the corresponding mRNA. Kinetic analysis of the GPx reaction suggested a tert-uni ping−pong mechanism, which involves peroxide mediated oxidation of the selenocysteine (*11*). Although the enzyme accepts reduced glutathione as hydrogen donor, protein thiols may also be used as reductants (*2*, *3*). A further peculiar property of GPx4, which distinguishes this enzyme from other GPx-isoforms, is its strong tendency toward protein polymerization (*2*, *3*, *5*). Unfortunately, the structural basis of the unique enzyme properties of GPx4 is not well understood, and this lack of knowledge is related to the absence of direct structural data on this enzyme. There are structural models for GPx4 (*12*, *13*), which are based on X-ray coordinates of other GPx-isoforms (*14*, *15*). Although the degree of amino acid conservation among GPx-isoforms is rather low, these models served as suitable tools to identify target amino acids for site-directed mutagenesis impacting catalytic activity (*11*,

[†] This work was supported in part by research grants from Deutsche Forschungsgemeinschaft (Ku 961/6-3), Sfb 498 (to N.K.) and the European Commission (FP6, LSHM-CT-2004-0050333).

[‡] The atomic coordinates and structure factors (pdb entry 2OBI) have been deposited in the Protein Data Bank, Research Collaboratory for Structural Bioinformatics, Rutgers University, New Brunswick, NJ (http://www.rcsb.org/).

[§] This paper is dedicated to Prof. H. Sies (Düsseldorf) on the occasion of his 65th birthday.

* To whom correspondence should be addressed. Tel: +49-30-450 528040. Fax: +49-30-450 528905. E-mail: hartmut.kuehn@charite.de.

[1] Abbreviations: GPx, glutathione peroxidase; GSH, glutathione; U, selenocysteine. The one letter code for amino acids is used throughout this article.

10.1021/bi700840d CCC: $37.00 © 2007 American Chemical Society
Published on Web 07/13/2007

16). Sequence alignments of GPx-isoforms indicated the conservation of three catalytically important amino acids (U46, Q81, and W136 in GPx4), and mutagenesis of this triad impaired enzymatic activity (*11*, *16*).

The major reason for the lack of direct structural information on GPx4 has been the absence of a highly effective natural enzyme source. Because large-scale expression of selenocysteine-containing proteins in recombinant systems is problematic (inefficient selenocysteine-incorporating machinery), we overexpressed the U46C mutant of human cytosolic GPx4 (c-GPx4) in *E. coli* (*17*). The recombinant enzyme was purified to electrophoretic homogeneity, crystallized, and used for X-ray diffraction studies. During the course of this work, X-ray coordinates for catalytically inactive U-to-G mutants of human GPx1 (pdb entry 2F8A) and GPx4 (pdb entry 2GS3) were deposited in the Protein Data Bank database. In addition, datasets for the U-to-C mutant of GPx2 (pdb entry 2HE3) and for selenium-free GPx5 (pdb entry 2I3Y) were also deposited, but the functional relevance of these structural data have not been explored.

Here, we report the crystal structure of the catalytically active U46C mutant of human GPx4 and test the functional importance of selected amino acids for catalysis and protein polymerization by multiple site-directed mutagenesis. Our data comprehensively describe the 3D structure of the enzyme to 1.55 Å and indicate the catalytic importance of C46, Q81, and W136. Moreover, we identified three surface exposed cysteine residues, which appear to be essential for protein polymerization.

MATERIALS AND METHODS

Chemicals. The chemicals used were from the following sources: EDTA, dithiiothreitol, NADPH, glutathione, glutathione reductase, and isopropyl-D-thiogalactopyranoside, Sigma (Deisenhofen, Germany); lysozyme, Fluka (Deisenhofen, Germany); sodium dodecylsulfate, imidazole, and Hybond-N nitrocellulose blotting membrane NC45, Serva (Heidelberg, Germany); PWO DNA Polymerase, agarose, ampicilline, and kanamycine, Boehringer Mannheim (Mannheim, Germany); restriction endonucleases, New England Biolabs GmbH (Schwalbach, Germany); bacto yeast extract, bacto agar, and bacto tryptone, Difco (Detroit, Michigan); and rainbow molecular mass markers, Amersham Life Science (Braunschweig, Germany).

Bacterial Expression and Purification of the U46C Mutant of Human Cytosolic GPx4. The cDNA encoding the human cytosolic GPx4 (c-GPx4) was amplified by RT-PCR, and the resulting fragment was ligated into the pQE-30 bacterial expression plasmid. The expression strategy was designed in such a way that the complete primary structure of the c-GPx4 (except the starting Met) was retained. An additional tail of 13 amino acids, which included a hexa-histidine-tag was introduced to allow effective purification. The final N-terminal sequence of the recombinant protein reads M-R-G-S-H-H-H-H-H-H-G-S-A-C. The last C corresponds to the initial M of the native enzyme. U46 was mutated to C employing the Quick-change mutagenesis kit (Invitrogen, Hilden, Germany), and the complete expression construct was sequenced. The recombinant mutant protein was then expressed in *E. coli* and purified from the bacterial lysis supernatant by consecutive steps of affinity chromatography on a Ni-agarose column and FPLC anion exchange chromatography. Details of the expression and purification procedures are given in Supporting Information (Figure S1).

Crystallization. The sparse matrix crystallization method (*18*) was applied to screen for optimal crystallization conditions. For the production of crystals, a solution of purified GPx4 (5.7 mg/mL) in 10 mM Tris/Cl buffer (pH 8.0) containing 1% glycerol and 5 mM TCEP was used. The enzyme was crystallized in hanging drops by the vapor diffusion method at 22 °C. The hanging drops were prepared by mixing 3 μL of the protein solution with 1 μL of the reservoir fluid containing the precipitating agents. Crystals of GPx4 were obtained when the reservoir solution contained 15% PEG 8000 in 0.1 M MES buffer (pH 6.5). Within 3−5 days, crystals grew to a maximum size of $0.1 \times 0.1 \times 0.4$ mm^3. An image of typically shaped crystals is given in Supporting Information (Figure S2).

X-Ray Data Collection, Structure Determination, and Refinement. X-ray data collection was performed at 100 K using a cryoprotectant consisting of 85% (v/v) reservoir solution and 15% glycerol. Diffraction data were collected at the synchrotron beamline BL14.1 of the Protein Structure Factory and Freie Universität Berlin at BESSY (Berlin, Germany) with a MAR225-MOSAIC detector. The crystal to detector distance was fixed at 150 mm. The rotation increment for each frame was 0.5° with an exposure time of 6 s. All data were indexed and processed using HKL2000 (*19*). The space group was $P3_121$ with unit cell dimensions of $a = b = 61.36$ Å, $c = 113.89$ Å, $\alpha = \beta = 90°$, and $\gamma = 120°$. The CCP4 program PHASER (*20*) was used to locate the molecular replacement solution using the model obtained from the structure of GPx1 (pdb entry 1GP1). Crystallographic refinements were performed using CNS (*21*) and the CCP4 program REFMAC (*22*). To create a test set that was used to calculate R_{free}, 5% of the reflections were randomly selected. Manual rebuilding of the GPx4 model and electron density interpretation was performed using O (*23*) and COOT (*24*). Positions of water molecules were identified with CNS and were also checked manually. With the final model, refinement converged at $R_{cryst} = 16.4\%$ and $R_{free} = 18.6\%$. The structure was validated with the programs PROCHECK (*25*) and WHAT_CHECK (*26*). All figures were created using PyMOL (*27*). Electrostatic calculations were performed with APBS (*28*).

Miscellaneous Methods. GPx4 activity was assayed spectrophotometrically, and the assay mixture consisted of 1 mL 0.1 M Tris/Cl buffer at pH 7.4, containing 5 mM EDTA, 0.1% Triton X-100, 0.2 mM NADPH, 3 mM glutathione, and 1 unit of glutathione reductase. Purified GPx4 mutants were added, and the mixture was preincubated at 37 °C for 5 min. Then the reaction was started by the addition of 25 μM *tert*-butyl hydroperoxide, and the decrease in absorbance at 340 nm was measured. (A molar extinction coefficient for NADPH of 6.22×10^3 $(M \times cm)^{-1}$ was used. Typical kinetic progress curves for selected GPx4 mutants are shown in Supporting Information (Figure S3). Protein concentration was determined using the BIO-RAD (Bio-Rad Laboratories GmbH, Munich, Germany) protein assay. SDS−PAGE was performed on pre-cast PAGE gradient gels (4−15%, Pharmacia FAST system). Site-directed mutagenesis was carried

out using the Quick-change mutagenesis kit (Invitrogen, Hilden, Germany), and all mutants were properly sequenced.

RESULTS

Crystal Structure of Cytosolic Human GPx4. The crystal structure of the human cytosolic GPx4, was refined to a resolution of 1.55 Å. A summary of important crystallographic parameters and refinement statistics are given in Supporting Information (Table S1). The established structural model characterizes GPx4 as a monomeric protein consisting of 170 amino acids. The affinity tag and the five most N-terminal amino acids of the natural enzyme could not be located because of weak electron density, suggesting a high degree of structural flexibility of this part of the molecule. The protein structure shows the typical thioredoxin motif (*29*) consisting of four α-helices that are localized at the protein surface and seven *β*-strands, five of which are clustered to form a central *β*-sheet (Figure 1A). The catalytic triad (*11*, *16*) consisting of C46[2], Q81, and W136 is localized at a flat impression of the protein surface. It extends into a positively charged surface exposed patch of basic amino acids (K48, K135, and R152), which also contains the polar T139 (Figure 1B). This structural motif is lined by apolar residues (M156, P155, G154, I129, L130, A133, I134, F78, and G79), and these amino acids may be involved in positioning hydrophobic lipid hydroperoxides at the active site. R152 is conserved in all GPx-isoforms, whereas K48, K135, and T139 are unique for GPx4. Interestingly, T139 is mutated to E in all other GPx-isoforms, and thus, this residue may be related to peculiar GPx4 properties. Q81 and W136 are in hydrogen-bond distance to C46 (Figure 1C), and this arrangement might be important for catalytic activity. In the native selenocysteine-containing GPx4, U46 has been suggested to be present as anion in the catalytically active form, and Q81 and W136 might sustain hydrogen bridges to the selenium to stabilize its deprotonated form. Our structural data support this hypothesis.

In addition to the catalytic triad, a similar structural motif consisting of C148, Q123, and W119 was detected on the protein surface opposite the catalytic center. The structural geometry of this pseudo-catalytic cluster resembles that of the active site, but the distances between the sulfur atom of C148 and its potential binding partners (Q123 and W119) are far too long to sustain effective hydrogen bridges (Figure 2). These data suggested the catalytic silence of the pseudo-catalytic cluster. In fact, site-directed mutagenesis (data not shown) does not provide any evidence for the catalytic importance of these amino acids.

Structural Comparison of GPx4 with Other GPx-Isoforms. As indicated above, GPx4 is unique among GPx-isoforms with respect to its broad substrate specificity and its strong tendency for protein polymerization. To explore the structural basis for these remarkable enzyme properties, we first compared the structures of various GPx isozymes (Figure 3). Multiple sequence alignments (Figure 3 A) indicated that GPx4 lacks an internal stretch of about 20 amino acids, which is present in other GPx-isoforms. In the 3D structure of other GPx isozymes, this sequence forms a surface exposed loop

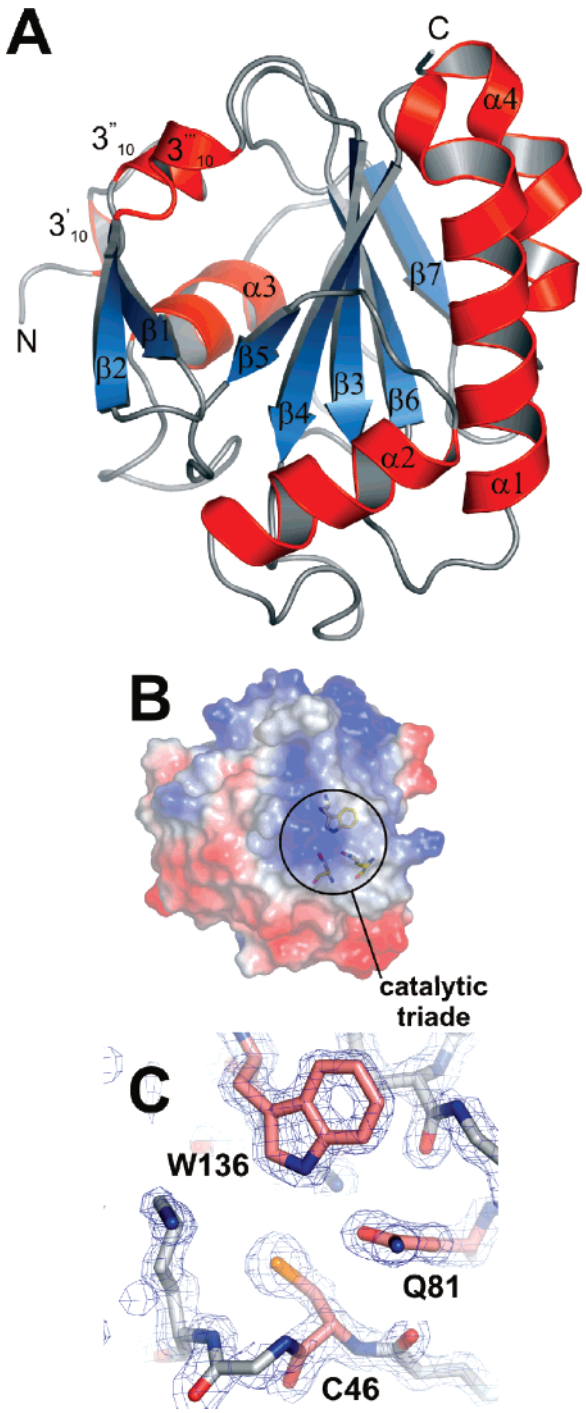

FIGURE 1: X-ray structural analysis of the U46C mutant of human cytosolic GPx4. Panel A: Scheme of the overall structure of GPx4 as a ribbon diagram. The α-helices and *β*-strands are numbered. Panel B: Electrostatic potential surface representation of the GPx4 molecule showing surface exposure of the catalytic triad C46, Q81, and W136 (circled region). Electrostatic surface potentials were calculated with the nonlinear Poisson−Boltzmann equation and are shown as a gradient from +3kT/e (blue) to −3kT/e (red). Panel C: 2 *Fo* − *Fc* electron density map of the catalytic triad contoured at 1.0*σ* above the mean density and colored in blue. C46, Q81, and W136 are shown as red sticks.

(loop 1) that does not exist in GPx4 (Figure 3B). Interestingly, this loop structure lines the active site of other GPx-isoforms and partially shields W136, a constituent of the catalytic triad (Figure 3C). It may be concluded that the existence of this loop structure limits the accessibility of complex lipid substrates to the active site of most GPx-

[2] C46 in our recombinant enzyme preparation corresponds to U46 in the native enzyme.

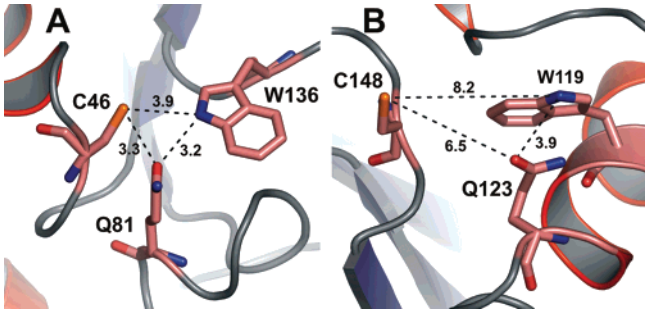

FIGURE 2: Comparison of the geometry of the catalytic triad with a similar structural motif (pseudo-catalytic center) located opposite the active site. Panel A: Active site structure of the U46C mutant of human GPx4. Panel B: Structure of the pseudo-catalytic center.

isoforms. In contrast, the lack of this structural element in GPx4 may allow the efficient binding of complex lipid molecules at the active site. Further comparison of selected GPx crystal structures revealed a second peculiarity of GPx4. In addition to loop 1, another surface feature, which is shared by GPx1, GPx2, and GPx5, is modified in GPx4. Amino acid alignments (Figure 3A) indicated the lack of six residues in GPx4, which are conserved in the other isoforms (loop 2). In the 3D structure, this amino acid deletion dislocates helix 2 (Figures 1A and 3B). In oligomeric GPx isoforms helix 2 and loop 1, which is lacking in GPx4, are constituents of the inter-monomer interface (*30*). Thus, modification of these surface structural elements may be regarded a structural reason for the monomeric character of GPx4. Because of the surface exposure of the active site, the oligomerization of the GPx isoform might impact the catalytic properties of the isoenzymes, in particular the substrate specificity.

Mutagenesis of Cysteine Residues with Potential Importance for Enzyme Polymerization. In oxidizing environments, GPx4 forms high molecular mass polymers, and this polymerization process has been implicated in sperm development (*5*). Other GPx-isoforms do not exhibit this tendency, but the structural basis for this differential behavior has not been explored in detail. Because surface exposed cysteines have been suggested to play a role, we first looked for the conservation of cysteines among GPx-isoforms. Our multiple sequence alignments (Figure 3A) indicated that among the cysteine residues present in GPx4 only C75 is conserved in other GPx-isoforms. This amino acid is localized in a region that is very similar in all GPx-isoforms but is not surface exposed. Neither of the other cysteine residues found in GPx4 is conserved in any other GPx isoform regardless of whether they are surface exposed (C10, C66, C107, and C148) or not (C37). It should be mentioned at this point that in addition to the above mentioned cysteines our expression construct contains two other cysteine residues in the N-terminal region. The starting methionine of the native enzyme was mutated to C (C1) to allow convenient cloning. The second amino acid in the native enzyme is also a cysteine (C2), and this residue was conserved during the cloning procedure. Unfortunately, the spatial localization C1 and C2 could not be defined because of weak electron density in this region of the protein molecule. These data suggest that the N-terminus of the protein is flexible, and thus, C1 and C2 are most probably surface exposed.

Mass spectral analysis of tryptic digest fragments of native GPx4 polymers suggested that U46 and C148 might play a major role in the polymerization process (*13*). To investigate the mechanism of GPx4 polymerization in more detail, we first tested the tendency of the U46C mutant to form protein polymers *in vitro*. For this purpose, we followed oligomer formation by turbidity assays and SDS−PAGE under non-reducing conditions. From Figure 4A, it can be seen that a clear solution of the U46C mutant turned turbid during aerobic incubation as indicated by the increase in absorbance at 600 nm. This increase in turbidity was paralleled by the formation of high molecular mass polymers (Figure 4C). Under reducing conditions (in the presence of 10 mM dithiothreitol), turbidity and polymer formation was prevented, and subsequent addition of a reductant to turbid GPx4 suspensions partly resolved the polymers (data not shown). These data confirmed the involvement of disulfide bridge formation in protein polymerization.

To test the relevance of the various surface exposed cysteines, we employed a complex mutagenesis strategy exchanging these residues separately and jointly with alanines (Figure 4A and B). The recombinant U46C mutant, which served as a starting target for this strategy, exhibited a strong tendency for polymerization, and a similar behavior was observed for the U46C+C107A and the U46C+C148A mutants. These results, which were confirmed by SDS−PAGE (Figure 4C), suggested that C107 and C148 might not be of major importance for protein polymerization. In contrast, the catalytically inactive U46A mutant was characterized by a strongly reduced polymerization tendency, and C10A+U46C and U46C+C66A hardly polymerized at all (Figure 4A). These results suggested that C10 and C66 are important for polymer formation. In previous studies on *in vivo* polymerization of native GPx4, U46 and C148 have been implicated as key players (*13*). However, the strong degree of enzyme polymerization of the U46C+C148A mutant (Figure 4A) was not consistent with this hypothesis. To further explore the role of C148, we created the U46A+C148A double mutant. If C148 could be important for protein polymerization, one would expect that polymerization of the U46A mutant would further be impaired when C148 is converted to A. However, we found that the U46A+C148A mutant exhibited polymerization behavior similar to that of the U46A single mutant (Figure 4B). For additional evidence of the role of C10, C46, and C66 in GPx4 polymerization, we next created quadruple (C10A+U46C+C66A+C148A) and quintuple (C10A+U46C+C66A+C107A+C148A) mutants, and as expected, we did not detect protein polymerization (Figure 4B and C). Taken together, these mutagenesis data suggest that C10, C66, and the catalytic C46 may be important for *in vitro* protein polymerization of the U46C GPx4 mutant. In contrast, C107 and C146 might not be of major relevance.

To understand the structural basis for the variable impact of various surface exposed cysteine residues on GPx4 polymerization, we searched our crystallographic data for areas of inter-monomer contacts within GPx4 crystals. Interestingly, we found that C10, C46, and C66 are located at monomer−monomer interfaces. In fact, the catalytically active C46 was localized in proximity (7−8 Å) to both C10 and C66 of adjacent monomers (Figure 5A). In contrast, C107 and C148 are truly solvent exposed and do not contact any part of the neighboring monomers (Figure 5B). If such monomer−monomer interaction also takes place in

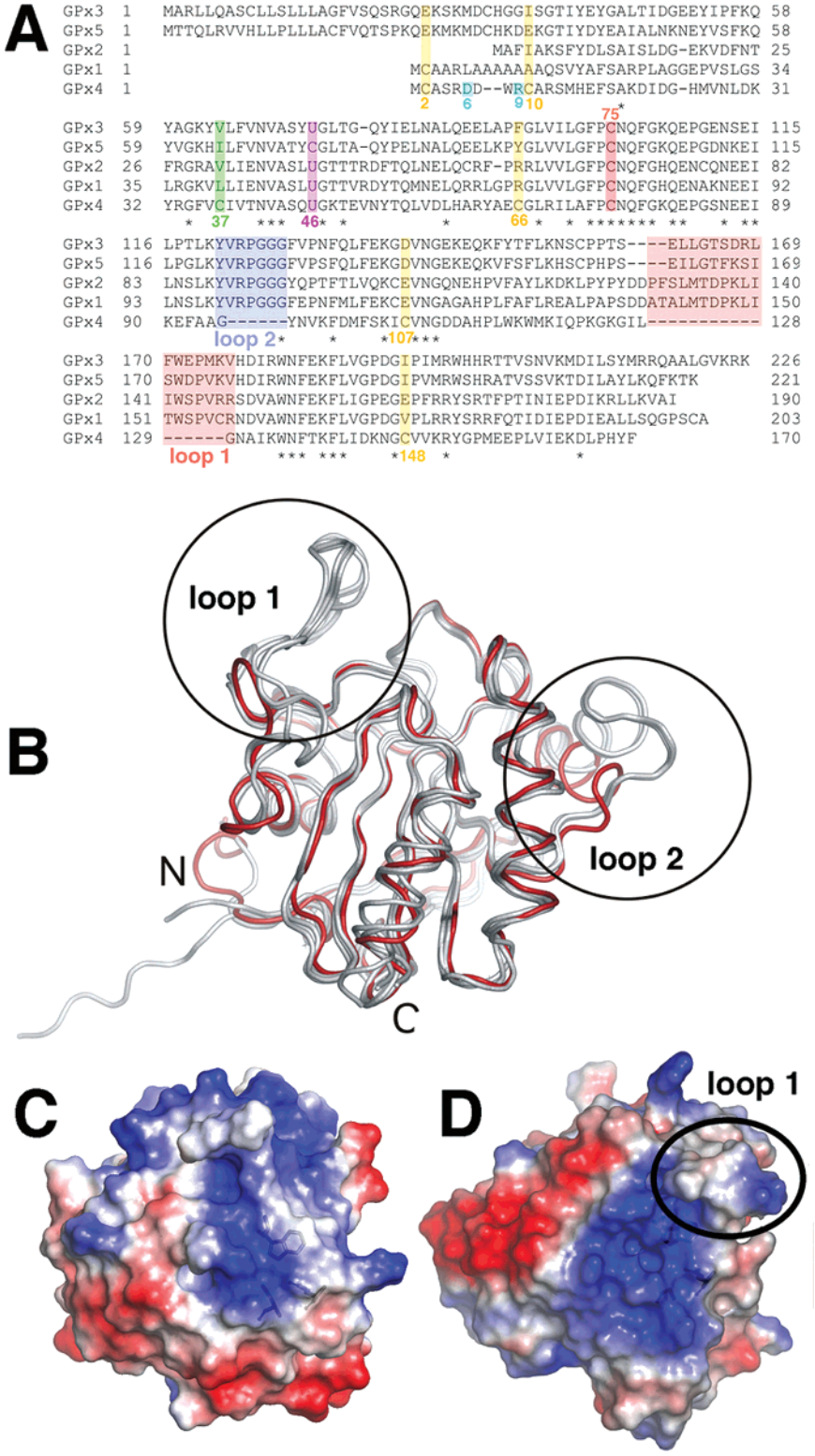

FIGURE 3: Structural comparison of GPx-isoforms. Panel A: Structure-based multiple amino acid alignment of various GPx-isoforms. The catalytic selenocysteine, which is mutated to either G or A in most crystal structures, is indicated in magenta. The conserved cysteine (C75 in GPx4) that is not surface exposed is shown in red. C37 of GPx4, which is neither conserved nor surface exposed, is indicated in green. The other cysteine residues of GPx4 (marked in yellow) are all surface exposed. Among them, only C10 and C66 appear to be involved in protein polymerization. The most N-terminal amino acids that show up in the crystal structure of GPx4 are indicated in turquoise (D6 for our structure (pdb entry 2OBI), K9 for pdb entry 2GS3). Panel B: Superposition of the protein backbone of various GPx-isoforms. The protein backbone of GPx1, GPx2, and GPx5 are shown in gray, and the backbone of GPx4 is indicated in red. The loop regions (loops 1 and 2), which are absent in GPx4, are indicated by circles. Panels C and D: Comparison of the surface structures of GPX4 (C) and GPx1 (D). The circle in panel D indicates loop 1, which partially shields the putative substrate-binding region of the enzyme. This loop is absent in GPx4, which may explain the broad substrate specificity of the enzyme.

aqueous solutions, a structural explanation for our polymerization results may be provided. It should, however, be stressed that a distance of 7−8 Å is rather large for the effective formation of inter-monomer disulfide bridges.

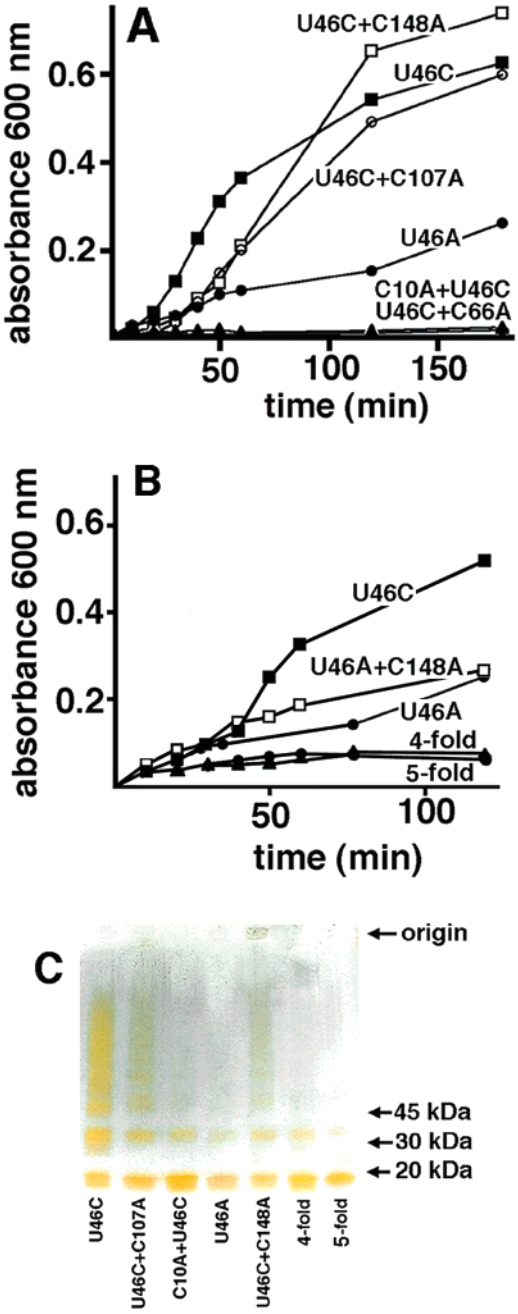

FIGURE 4: Protein polymerization of GPx4 mutants. The mutant GPx4 species were expressed, purified, and subjected to turbidity assays and SDS−PAGE. Panels A and B: Oligomer formation (increase in absorbance at 600 nm) of GPx4 mutants, testing the importance of surface exposed cysteine residues. The overlapping traces at the bottom of panel A indicate the low polymerization tendency of the C10A+U46C and U46C+C66A mutants. Similarly, the quadruple and quintuple mutants (bottom of panel B) hardly polymerize. Panel C: SDS−PAGE under non-reducing conditions (silver staining). The high molecular mass smears indicate the formation of enzyme polymers. Enzyme dimers show up at a molecular mass of about 35 kDa.

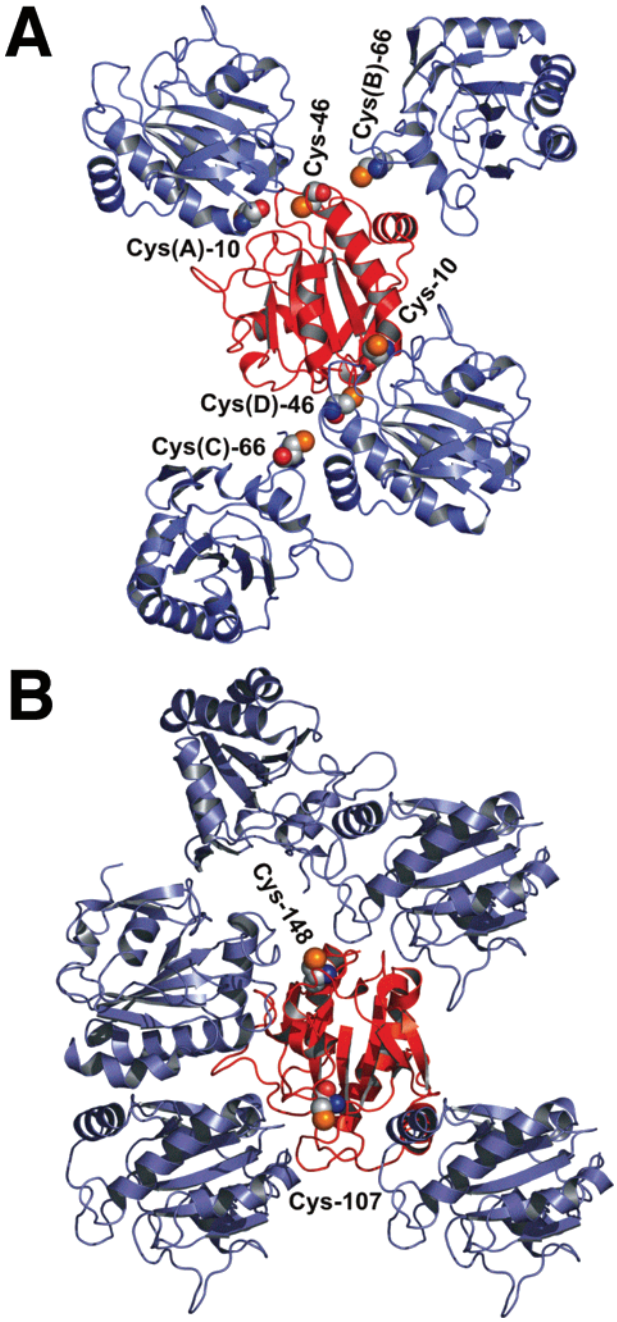

FIGURE 5: Monomer−monomer interfaces for the potential formation of the intermolecular disulfide-bridge as seen in the crystal lattice. Panel A: Spatial proximity of the three surface exposed cysteines C10, C46, and C66 (spheres) in neighboring GPx4 monomers. These residues are exposed at the surface of the monomers but are shielded in the crystals owing to inter-monomer contacts. For clarity reasons, a selected monomer (red) is shown with only four surrounding monomeric partners (A−D, shown in blue). These partners were selected out of a total of five symmetry mates, which are in crystal contact with the central (red) monomer. Panel B: Crystal environment of the two surface accessible cysteine residues C107 and C148 (spheres). In this image, one selected monomer (red) is surrounded by four selected symmetry mates (blue). It can be seen that C107 and C148 have no potential partner for the formation of inter-monomer disulfide-bridges within the crystal lattice.

However, minor site chain rearrangements may shorten this distance, and such dynamic alterations appear possible in aqueous solution.

Mutagenesis of the Catalytic Triad. To test the catalytic relevance of the suggested catalytic triad (*11*, *16*), we performed multiple site directed mutagenesis. Previous results indicated that the U46C GPx4 mutant only exhibits about 1% of residual activity when compared with that of the native enzyme (*16*). This result was not surprising because selenocysteine is more acidic than cysteine, and thus, the catalytically active ionized form is more abundantly available at neutral pH. We found that under our experimental conditions the U46C mutant exhibits a molecular turnover

Table 1: Catalytic Activity of GPx4 Active Site Mutants

enzyme variant	molecular turnover (s^{-1})	rel. catalytic activity
U46C	0.025 ± 0.002	100%
U36A	0	0%
U46C+Q81E	0.004 ± 0.002	16%
U46C+Q81N	0.005 ± 0.005	20%
U46C+Q81L	0.004 ± 0.005	16%
U46C+W136H	0.002 ± 0.002	8%
U46C+W136F	0.003 ± 0.005	12%

[a] The recombinant mutant GPx4 species were expressed in *E. coli* and purified to homogeneity by affinity chromatography on Ni-agarose and subsequent mono-Q FPLC. Pure enzyme preparations were then subjected to activity assays ($n = 3$). The mean $\pm$ SD values are given.

rate of 0.025 ± 0.002 s^{-1}. When we tested the C46A mutant, no catalytic activity was measured (Table 1), which is consistent with the hypothesis that a redox-inactive residue such as alanine at this critical position leads to a complete loss in catalytic activity. Next, we mutated Q81 to E, N, and L and found strongly reduced catalytic activity for all mutants (Table 1). Finally, we replaced W136 with H and F. Here again, the resulting mutants exhibited only minor residual catalytic activity. Taken together, these data indicate that C46, Q81, and W136 are important for the residual catalytic activity of our U46C mutant.

DISCUSSION

Among selenium-containing glutathione peroxidases, GPx4 is peculiar because of its ability to reduce complex lipid hydroperoxides (*4*), its tendency toward polymerization (*5*), and its multiple functionality (*2*, *3*). As an anti-oxidative enzyme, it has been implicated in oxidation defense, apoptosis regulation, and modulation of eicosanoid biosynthesis (*2*, *3*). As a structural protein, it appears to be involved in the formation of the mitochondrial capsule during sperm development (*5*), and for this function, the formation of high molecular mass polymers appears to be important. The structural biology of GPx-isoforms in general and of GPx4 in particular has not been well investigated in the past. The structural models for GPx4 (*12*, *13*), which were constructed on the basis of the X-ray coordinates of other GPx-isoforms (*14*, *15*), adequately describe the secondary structural elements of the enzyme and the approximate localization of the catalytic triade. However, crystal structures now allow more detailed conclusions on the structural basis for the monomeric character of GPx4 and its broad substrate specificity.

The major reasons for the low abundance of direct structural data were the problems associated with recombinant expression of mammalian selenocysteine-containing proteins in prokaryotic and eukaryotic expression systems. Selenocysteine is encoded by a UGA opal codon, which signals the stop of protein synthesis in most recombinant expression systems. However, in mammalian cells, translational termination is prevented by the selenocysteine insertion sequence localized in the 3′-untranslated region of the corresponding mRNA. The molecular mechanism of the suppression of translational termination has not been completely clarified, but the binding of regulatory proteins to the 3′-UTR appears to be involved. To circumvent the problems associated with the recombinant expression of selenoproteins, two selenium-containing GPx-isoforms (GPx1 and GPx3) have been purified in sufficient amounts from natural sources, and their crystal structures have been published some years ago (*14*, *15*). More recently, four high-resolution structures for various selenium-free recombinant GPx mutants (GPx1, pdb entry 2F8A, 1.5 Å; GPx2, pdb entry 2HE3, 2.1 Å; GPx4, pdb entry 2GS3, 1.9 Å; GPx5, pdb entry 2I3Y, 2.0 Å) have been deposited in the Protein Data Bank, but the functional relevance of these structural data has not been investigated. Here, we report for the first time the crystal structure of the catalytically active U46C mutant of human cytosolic GPx4. In addition, we tested by site-directed mutagenesis the functional importance of selected amino acids for enzyme activity and protein polymerization. To identify target amino acids, we first performed structure-based alignments of various GPx-isoforms. When we compared the recently submitted pdb data for the U46G mutant of human GPx4 (pdb entry 2GS3) with our results, we found that the overall structures were similar, but the following differences should be mentioned: (i) The 2GS3 coordinates describe the structure of a catalytically inactive enzyme species (U46G), whereas our data characterize an active enzyme (U46C). (ii) Our data allowed a molecular resolution of 1.55 Å in comparison to 1.9 Å for 2GS3. (iii) In both structures, the N-terminal amino acids could not be detected. The most N-terminal residue visible in our dataset is D6. In contrast, the 2GS3 structure starts with R9.

During sperm development, native GPx4 undergoes protein polymerization, and the formation of disulfide bonds between surface exposed cysteine residues has recently been implicated (*19*). For other GPx-isoforms, such protein polymerization has not been described. To explore the structural basis for the differential polymerization behavior, we first performed multiple sequence alignments of various GPx-isoforms and found that neither of the surface exposed cysteines of GPx4 is conserved in any of the other GPx-isoforms (Figure 3). These data may explain the lack in tendency toward protein polymerization of other GPx-isoforms. However, our mutagenesis studies (Figure 4) indicated that the catalytically inactive U46A mutant exhibited a reduced polymerization tendency, suggesting that this amino acid may be important for polymerization (*13*). An even more pronounced reduction of enzyme polymerization was observed for the C10A+U46C and the U46C+C66A mutants, suggesting a key role for C10 and C66 in protein polymerization. However, we did not obtain any evidence for the involvement of surface exposed C107 and C148. If one translates these *in vitro* data to the *in vivo* situation, one can conclude that for polymerization of the native GPx4 that contains a more redox-reactive selenocysteine U46 might be an important player in the polymerization process. However, for the formation of mixed selenocysteine-cysteine bonds, binding partners are required, and their spatial arrangements must allow efficient covalent cross-linkage. In this context, it might be of particular importance that in our crystal structure U46 of one enzyme monomer comes close to C10 or C66 of adjacent monomers (Figure 5) and this arrangement is consistent with the our hypothesis that enzyme monomers are covalently linked together via the direct interactions of C46 with C10 or C66.

Previous mass spectral analysis of tryptic digest fragments obtained from GPx4 polymers and structural modeling of the polymerization process suggested the importance of the catalytic U46 and of C148 for polymer formation. It should be stressed at this point that involvement of two reactants (U46 and C148) only allows the formation of linear GPx4 polymers (*13*). However, the physicochemical properties of the mitochondrial capsule material do rather suggest a 3D network, and more recent investigations on the mechanism of mitochondrial capsule formation suggested the involvement of other structural proteins such as the sperm mitochondrion-associated cysteine-rich protein and keratin isoforms (*31*). We found that in addition to U46 (C46 in our mutant protein), two surface exposed cysteine residues (C10 and C66) are involved in the polymerization process, and this situation will allow the formation of a 3D network for GPx4 polymers. More detailed information on the mechanism of the polymerization process may be provided by direct structural investigation of GPx4 polymers. Polymer availability is not a limiting factor because large amounts of these aggregates can be prepared just by aerobic incubation of the purified monomers in the absence of reductive protection. However, the critical problem for such studies is that polymerization does not proceed in a synchronized manner, which leads to a complex mixture of GPx4 polymers with variable molecular masses. Moreover, there may even be a mixture of linear and 3D polymers, and such heterogeneous mixtures are difficult to evaluate.

ACKNOWLEDGMENT

We thank Gordon Winter for his support during data collection and Uwe Müller and the scientific staff of the Protein Structure Factory and the Freie Universität Berlin at beamlines BL 14.1 and BL 14.2 at BESSY (Berlin, Germany) for their continuous support of the project.

SUPPORTING INFORMATION AVAILABLE

Information on recombinant expression, purification, and crystallization of GPx4 as well as a description of the activity assay, data collection details, and refinement statistics. This material is available free of charge via the Internet at http://pubs.acs.org.

REFERENCES

1. Burk, R. F., and Hill, K. E. (1993) Regulation of selenoproteins, *Annu. Rev. Nutr. 13*, 65−81.
2. Brigelius-Floheh, R. (1999) Tissue-specific functions of individual glutathione peroxidases, *Free Radical Biol. Med. 27*, 951−965.
3. Imai, H., and Nakagawa, Y. (2003) Biological significance of phospholipid hydroperoxide glutathione peroxidase (PHGPx, GPx4) in mammalian cells, *Free Radical Biol. Med. 34*, 145−169.
4. Sattler, W., Maiorino, M., and Stocker, R. (1994) Reduction of HDL- and LDL-associated cholesterylester and phospholipid hydroperoxides by phospholipid hydroperoxide glutathione peroxidase and Ebselen (PZ 51), *Arch. Biochem. Biophys. 309*, 214−221.
5. Ursini, F., Heim, S., Kiess, M., Maiorino, M., Roveri, A., Wissing, J., and Flohe, L. (1999) Dual function of the selenoprotein PHGPx during sperm maturation, *Science 285*, 1393−1396.
6. Nomura, K., Imai, H., Koumura, T., Arai, M., and Nakagawa, Y. (1999) Mitochondrial phospholipid hydroperoxide glutathione peroxidase suppresses apoptosis mediated by a mitochondrial death pathway, *J. Biol. Chem. 274*, 29294−29302.
7. Borchert, A., Wang, C. C., Ufer, C., Schiebel, H., Savaskan, N. E., and Kuhn, H. (2006) The role of phospholipid hydroperoxide glutathione peroxidase (GPx4) isoforms in murine embryogenesis, *J. Biol. Chem. 281*, 19655−19664.
8. Imai, H., Suzuki, K., Ishizaka, S., Ichinose, S., Oshima, H., Okayasu, I., Emoto, K., Umeda, M., and Nakagawa, Y. (2001) Failure of the expression of phospholipid hydroperoxide glutathione peroxidase in the spermatozoa of human infertile males, *Biol. Reprod. 64*, 674−683.
9. Diaconu, M., Tangat, Y., Böhm, D., Kühn, H., Michelmann, W., Schreiber, G., Haidl, G., Glander, J. H., Engel, W., and Nayernia, K. (2006) Failure of phospholipid hydroperoxide glutathione peroxidase expression in oligoasthenozoospermia and mutations in the PHGPx gene, *Andrologia 38*, 152−157.
10. Roveri, A., Maiorino, M., Nisii, C., and Ursini, F. Purification and characterization of phospholipid hydroperoxide glutathione peroxidase from rat testis mitochondrial membranes, *Biochim. Biophys. Acta 1208*, 211−221.
11. Maiorino, M., Aumann, K. D., Brigelius-Flohe, R., Doria, D., van den Heuvel, J., McCarthy, J., Roveri, A., Ursini, F., and Flohe, L. Probing the presumed catalytic triad of selenium-containing peroxidases by mutational analysis of phospholipid hydroperoxide glutathione peroxidase (PHGPx), *Biol. Chem. Hoppe-Seyler 376*, 651−660.
12. Brigelius-Flohe, R., Schomburg, D., and Flohe, L. Glutathione peroxidase revisited: simulation of the catalytic cycle by computer-assisted molecular modeling, *Biomed. Environ. Sci. 10*, 136−515.
13. Mauri, P., Benazzi, L., Flohe, L., Maiorino, M., Pietta, P. G., Pilawa, S., Rovery, A., and Ursini, F. (2003) Versatility of selenium catalysis in PHGPx unraveled by LC/ESI-MS/MS, *Biol. Chem. 384*, 575−588.
14. Epp, O., Ladenstein, R., and Wendel, R. (1983) The refined structure of the selenoenzyme glutathione peroxidase at 0.2 nm resolution, *Eur. J. Biochem*, *133*, 51−69.
15. Ren, B., Huang, W., Akesson, B., and Ladenstein, R. (1997) The crystal structure of selenoglutathione peroxidase from human plasma at 2.9 Å resolution, *J. Mol. Biol. 268*, 869−885.
16. Maiorino, M., Aumann, K. D., Brigelius-Flohe, R., Doria, D., van den Heuvel, J., McCarthy, J., Roveri, A., Ursini, F., and Flohe, L. (1998) Probing the presumed catalytic triade of selenium-containing peroxidases by mutational analysis, *Ernährungswiss. 37*, 118−121.
17. Schnurr, K., Borchert, A., Gerth, C., Anton, M., and Kuhn, H. (2000) Bacterial and non-bacterial expression of wild-type and mutant human phospholipid hydroperoxide glutathione peroxidase and purification of the mutant enzyme in the mg-scale, *Protein Expression Purif. 19*, 403−410.
18. Jancarik, J., and Kim, S.-H. (1991) Sparse matrix sampling: a screening method for crystallization of proteins, *J. Appl. Crystallogr. 24*, 409−411.
19. Otwinowski, Z., and Minor, W. (1997) Processing of X-ray diffraction data collected in oscillation mode, *Methods Enzymol. 276*, 307−326.
20. McCoy, A. J., Grosse-Kunstleve, R. W., Storoni, L. C., and Read, R. J. (2005) Likelihood-enhanced fast translation functions, *Acta Crystallogr., Sect. D 61*, 458−464.
21. Brünger, A. T., Adams, P. D., Clore, G. M., DeLano, W. L., Gros, P., Grosse-Kunstleve, R. W., Jiang, J. S., Kuszewski, J., Nilges, M., Pannu, N. S., Read, R. J., Rice, L. M., Simonson, T., and Warren, G. L. (1998) Crystallography and NMR system: a new software suite for macromolecular structure determination, *Acta Crystallogr., Sect. D 54*, 905−921.
22. Collaborative Computational Project, Number 4. (1994) The CCP4 suite: programs for protein crystallography, *Acta Crystallogr., Sect. D 50*, 760−763.
23. Jones, T. A., and Kjeldgaard, M. (1997) Electron-density map interpretation, *Methods Enzymol. 277*, 173−208.
24. Emsley, P., and Cowtan, K. (2004) Coot: model-building tools for molecular graphics, *Acta Crystallogr., Sect. D 60*, 2126−213.
25. Laskowski, R. A., MacArthur, M. W., Moss, D. S., and Thornton, J. M. (1993) PROCHECK: a program to check the stereochemical quality of protein structures, *J. Appl. Crystallogr. 26*, 283−291.
26. Hooft, R. W., Vriend, G., Sander, S., and Abola, E. E. (1996) Errors in protein structures, *Nature 381*, 272.
27. DeLano, W. L. (2002) *The PyMOL Molecular Graphics System*, DeLano Scientific, San Carlos, CA. http://www.pymol.org.

28. Baker, N. A., Sept, D., Joseph, S., Holst, M. J., and McCammon, J. A. (2001) Electrostatics of nanosystems: Application to microtubules and the ribosome, *Proc. Natl. Acad. Sci. U.S.A. 98*, 10037−10041.
29. Martin, J. L. (1995) Thioredoxin: a fold for all reasons, *Structure 3*, 245−250.
30. Maiorino, M., Ursini, F., Bosello, V., Toppo, S., Tosatto, S. C., Mauri, P., Becker, K., Roveri, A., Bulato, C., Benazzi, L., dePalma, A., and Flohé, L. (2007) The thioredoxin specificity of Drosophila GPx: A paradigm for a peroxiredoxin-like mechanism of many glutathione peroxidases, *J. Mol. Biol. 365*, 1033−1046.
31. Maiorino, M., Roveri, A., Benazzi, L., Bosello, V., Mauri, P., Toppo, S., Tosatto, S. C., and Ursini, F. (2005) Functional interaction of phospholipid hydroperoxide glutathione peroxidase with sperm mitochondrion-associated cysteine-rich protein discloses the adjacent cysteine motif as a new substrate of the selenoperoxidases, *J. Biol. Chem. 280*, 38395−38402.

BI700840D